Near-Infrared photometry of Neptune's small regular satellites with Keck

Mallory Helfenbein, Edward M. Molter, Imke de Pater, Damya Souami

Icarus 413 (2024) 116004

Contents lists available at ScienceDirect

Icarus

journal homepage: www.elsevier.com/locate/icarus

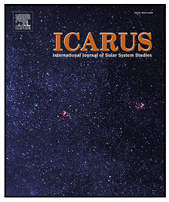

Research Paper

Near-Infrared photometry of Neptune's small regular satellites with Keck

Mallory Helfenbein [a,*], Edward M. Molter [b], Imke de Pater [c,b], Damya Souami [d,b,e]

[a] University of California, Berkeley, CA 94720, USA
[b] Department of Earth and Planetary Science, University of California, Berkeley, CA 94720, USA
[c] Department of Astronomy, University of California, Berkeley, CA 94720, USA
[d] LESIA, Observatoire de Paris, Université PSL, CNRS, Sorbonne Université, Université de Paris, 5 place Jules Janssen, F-92195 Meudon, France
[e] naXys, Department of Mathematics, University of Namur, Rue de Bruxelles 61, 5000 Namur, Belgium

ARTICLE INFO

Keywords:
Adaptive optics
Infrared photometry
Neptunian satellites
Albedo

ABSTRACT

We present data and images that provide insight on the infrared photometry and reflectivity of five of Neptune's small, regular moons: Proteus, Despina, Galatea, Larissa, and Naiad. Data were taken in the H-band (1.485–1.781 μm) on October 07, 2021 from the Keck telescope on Maunakea, Hawaii using the NIRC2 instrument with adaptive optics. We applied a shift-and-stack procedure that allowed us to enhance the signal to noise ratio on each moon as it moved across the detector frame-by-frame. We applied an aperture photometry method to these stacked images in order to extract the flux density and reflectivity of each moon. We find that the H-band albedo of Proteus, Larissa, Galatea, and Despina is the same within one standard deviation, with values near 0.13. The brightness of Naiad is somewhat lower, with a geometric albedo of 0.072 ± 0.013. Comparing these findings with previous observations at visible and infrared wavelengths, we find that four of the five observed moons display a slight spectral reddening from visible to near-infrared wavelengths.

1. Introduction

The Neptunian system was imaged in detail by *Voyager* 2 in 1989. Although there was only a single flyby of the planet, a wealth of information was obtained on both the planet itself and its rings and satellites (Smith et al., 1989). Six small, regular satellites within 5 planetary radii were detected: Proteus, Larissa, Despina, Galatea, Thalassa, and Naiad, Proteus being the largest and Naiad the smallest. Their visible-wavelength albedos appeared similar to those of the Uranian small satellites (Thomas and Veverka, 1991; Karkoschka, 2003). The *Voyager* 2 data were also used to determine the satellites' orbits (Jacobson, 1990; Owen et al., 1991).

Over the past three decades, advances in ground-based instrumentation and the deployment of the Hubble Space telescope (HST) have permitted further characterization of the Neptunian circumplanetary system. For example, the development of the anti-blooming CCD enabled the first observations of Proteus from the ground (Colas and Buil, 1992).

Using the NICMOS camera aboard HST, Dumas et al. (2002) performed photometry on Proteus, Galatea, Despina, and Larissa, though the spectral slope between the *Voyager* and NICMOS data remained inconclusive for all the satellites except Proteus. Thanks to developments in adaptive optics (AO) in the past few decades, the color and albedos of Neptune's inner satellites were further improved. By combining *Voyager* and near-infrared data, both Proteus and Galatea revealed a slight reddish color (Trilling and Brown, 2000; Dumas et al., 2002; de Pater et al., 2005; Renner et al., 2014; Molter et al., 2019).

The physical properties of these satellites provide useful constraints on several open questions in planetary science and in the study of protoplanetary discs. Several studies focusing on the dynamical history of the neptunian inner system use the observed physical properties of the satellites as constraining data (Banfield and Murray, 1992; Zhang and Hamilton, 2007, 2008). Some of the satellites have been shown to play an important role in the confinement of Neptune's rings arcs, as shown by the numerous studies on the topic (Goldreich et al., 1986; Porco, 1991; Salo and Hanninen, 1998; Namouni and Porco, 2002; Renner et al., 2014; Showalter et al., 2017; Giuliatti Winter et al., 2020; Souami et al., 2022, and references therein). The composition of Neptune's circumplanetary material also has implications for the formation history of the ice giants (e.g. Tiscareno and Murray, 2018), and the physics governing the scattering phase function of airless solar system bodies remains an area of active research (e.g. Déau et al., 2009). Our H-band photometry offers insights into the scattering phase function by providing new measurements of Neptune's moons. Thus allowing a description of the reflectivity of a surface as a function of the Sun-target-observer (S-T-O) phase angle and acting as an indicator of surface roughness (Karkoschka, 2001; Paradis et al., 2023).

* Corresponding author.
E-mail address: malloryhelfenbein@berkeley.edu (M. Helfenbein).

https://doi.org/10.1016/j.icarus.2024.116004
Received 7 November 2023; Received in revised form 29 January 2024; Accepted 14 February 2024
Available online 15 February 2024

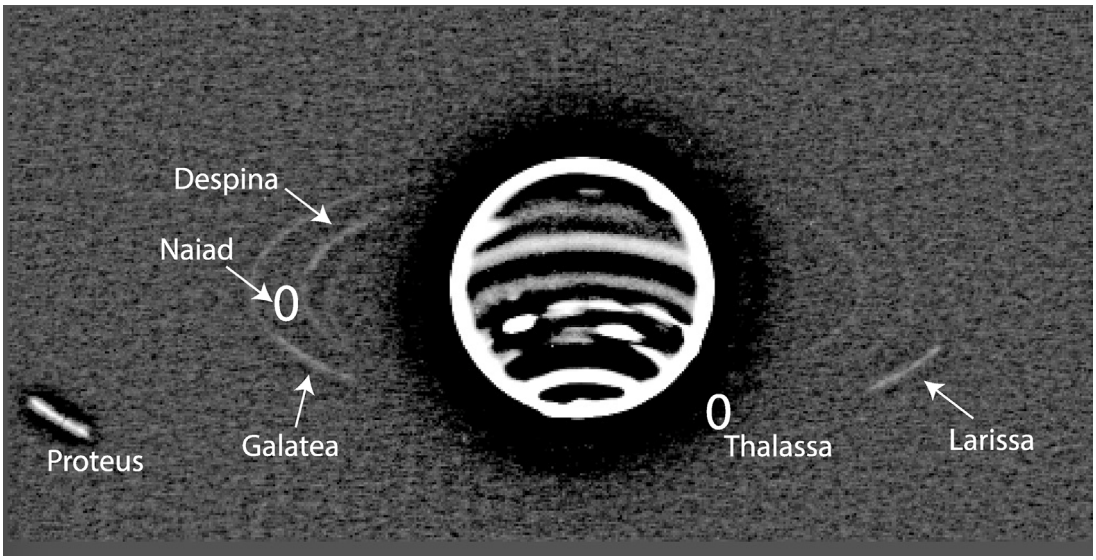

Fig. 1. A high-pass filtered image of Neptune, its ring system and satellites after stacking all 30 frames. The moons appear as arcs due to their motion on the sky. Naiad cannot be seen in individual frames, and Thalassa is too close to Neptune to be visible.

In this paper we present H-band (1.63 μm) photometry of Proteus, Galatea, Despina, Larissa, and Naiad.

2. Observations and data reduction

2.1. Data collection

We observed Neptune's moons on UT Oct 7, 2021 using the NIRC2 narrow camera (1024 × 1024 Aladdin-3 InSb array) coupled with the Adaptive Optics (AO) system (Wizinowich et al., 2000, 2004; van Dam et al., 2004) at Keck Observatory atop Maunakea, Hawaii. Our dataset consists of 30 one-minute exposures in H-band (1.485–1.781 μm) taken between 8:37 and 9:19 UT, centered on the planet Neptune, using Neptune itself for wavefront sensing. Standard near-infrared data reduction techniques were applied to each frame, including sky subtraction, cosmic ray removal, and flat-fielding. The images were photometrically calibrated using the standard star FS2[1] (Hawarden et al., 2001), which gave us a factor of 1.059×10^{-16} to convert the measurements in units of counts s^{-1} to erg s^{-1} cm^{-2} μm^{-1}. Fig. 1 shows an image of the system after summing all 30 frames. The image was high-pass filtered to avoid light contamination of the planet.

In order to retrieve accurate measurements of the flux densities of each of the moons, individual 60-s frames were shifted according to the expected position of the moon relative to Neptune's center and then co-added. The expected orbital positions were taken from the JPL Horizons system[2] (Giorgini, 2011), accessed using the `Astroquery` Python package (Ginsburg et al., 2019). Our shift-and-stack procedure makes use of the `Astropy`-affiliated `image_registration` Python package[3] first to align the planet Neptune across all the frames and then to apply the known x, y offsets of the moon at sub-pixel accuracy. In Fig. 2, we show the detection of each moon from the stacked frames.

2.2. Flux density measurements

In order to get accurate flux density measurements, we performed aperture photometry on the stacked frames. As first described by Gibbard et al. (2005), it is necessary to account for the missing flux in the wings of the point-spread function (PSF) when performing photometry on low signal-to-noise point sources (see also, e.g. de Pater et al., 2014; Molter et al., 2019). We follow the procedure described in Appendix and taken from Paradis et al. (2019, 2023) to determine the intensities of each moon. Our final derived flux densities are given in Table 1. We translated these fluxes into units of I/F using the equation (Hammel et al., 1989):

$$\frac{I}{F} = \frac{r^2 F_s}{\Omega F_\odot}, \tag{1}$$

where r is the satellite's heliocentric distance (29.922 AU) and $\pi F_\odot$ is the Sun's flux density at Earth's orbit (Colina et al., 1996). The solid angle under which we view the moon is

$$\Omega = \frac{\pi a' b'}{d^2}, \tag{2}$$

where a' and b' are the sky-projected radii of the moon in km assuming an ellipsoidal shape, and d is the geocentric distance (29.000 AU). The I/F is a measure of the sunlight-reflecting surface of each moon compared with a theoretical surface of the same size and distance that reflects the sunlight perfectly, referred to as the Lambertian reflector.

In order to translate the 3-dimensional triaxial ellipsoid shape of each moon given by Karkoschka (2003) into a sky-projected 2-dimensional area, we assume that the moons are rotating synchronously like Jupiter's small moons Amalthea, Thebe, Metis, and Adrastea (Smith et al., 1979; Thomas et al., 1998; Porco et al., 2003). In synchronous rotation, the smallest axis c of the satellite is orthogonal to the satellite's orbit plane and the longest axis is parallel to the vector pointing from the satellite to the planet (Goldreich and Peale, 1966; Peale, 1999), meaning that the satellite's projected area is maximized in a pole-on view and minimized in an equator-on view with a sub-observer longitude near 0° or 180°. At intermediate angles, the projected area is found by re-projecting the 3-D ellipsoid into the observer's plane according to the sub-observer latitude and longitude given by the JPL Horizons system. A summary of our results, including the observed flux, sub-observer latitude and longitude, projected area, and I/F of each moon are shown in Table 1.

3. Discussion

The reflectivities we measured are compared with other studies in Fig. 3 and Table 2. Table 2 presents a comprehensive review of all reflectivity measurements for the five moons considered in this study.

[1] https://www2.keck.hawaii.edu/inst/nirc/UKIRTstds.html.
[2] https://ssd.jpl.nasa.gov/horizons/app.html#/.
[3] https://github.com/keflavich/image_registration.

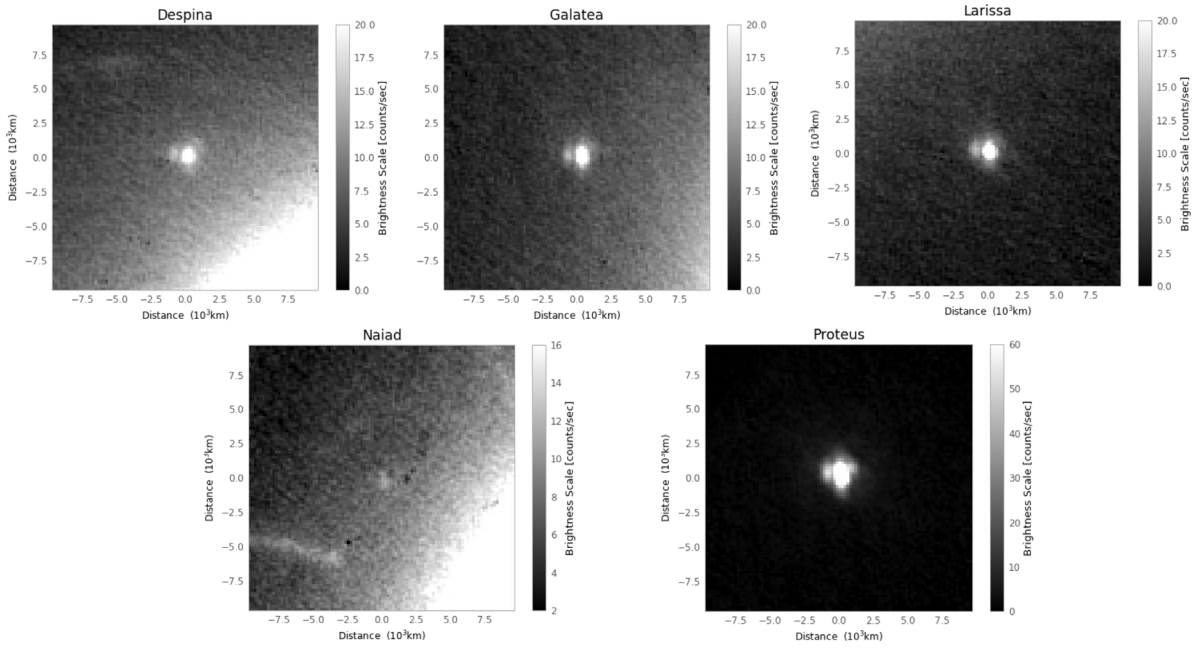

Fig. 2. Final stacked images of the 5 satellites, where the contrast of each image is enhanced to improve visibility. The extended morphology of the moons is due to the wings of the point spread function and is a part of the Airy pattern. The bar on the right of each image shows the linear intensity scale of each image. The distance scale is based on the observer-Neptune distance given by JPL Horizons at the time of observation, which comes out to 194 km/pixel.

Table 1
Final results shown above, including the calculated flux of each moon and the reflectivity value (I/F) calculated using the area of each moon. The radii values used to calculate the projected area were taken from Karkoschka (2003), and the sub-observer longitudes and latitudes are the average over the duration of the observation, taken from JPL Horizons. The uncertainty in the I/F value combines the uncertainty due to the RMS noise in the image, the flux calibration, and the flux bootstrapping uncertainties, and is the same percentage for the flux (see Appendix). The signal-to-noise ratio (SNR) was computed using the moon's uncertainty due only to the RMS noise in the image (see Appendix).

Moon unit	A_{proj} km^2	Radius km	(ob_lat, ob_lon) degrees	Flux erg s^{-1} cm^{-2} μm^{-1}	I/F	SNR	RMS noise erg s^{-1} cm^{-2} μm^{-1}
Despina	16 700	90 × 74 × 64	(−22.8, 136)	$8.02 \cdot 10^{-15}$	0.105 ± 0.0105	120	$3.89 \cdot 10^{-18}$
Galatea	22 600	102 × 92 × 72	(−22.8, 43.9)	$1.10 \cdot 10^{-14}$	0.106 ± 0.00993	210	$2.91 \cdot 10^{-18}$
Larissa	28 800	108 × 102 × 84	(−22.9, 299)	$1.39 \cdot 10^{-14}$	0.105 ± 0.0096	290	$2.74 \cdot 10^{-18}$
Proteus	137 000	218 × 208 × 201	(−26.6, 57.2)	$7.15 \cdot 10^{-14}$	0.114 ± 0.0104	1500	$2.71 \cdot 10^{-18}$
Naiad	3820	48 × 30 × 26	(−26.9, 287)	$1.07 \cdot 10^{-15}$	0.0608 ± 0.00725	20	$2.83 \cdot 10^{-18}$

To translate our I/F values into a geometric albedo, we assumed that Neptune's moons have the same phase curve at 1.6 μm as the better-studied Uranian Portia Group at visible wavelengths by *Voyager*, as presented by Karkoschka (2001). Unfortunately, direct observations of phase curves in the Neptunian system are unavailable; however, the similarity in both visible and near-infrared albedo between the Neptunian and the Uranian moons (Paradis et al., 2023) along with the agreement between the infrared phase angle derived by Paradis et al. (2023) and the visible wavelength curves makes this assumption at least somewhat reasonable. The Sun–Neptune-observer phase angle at the time of observation was 0.74°, which means the phase angle correction was ≈1.13.

The I/F values in Table 2 derived by other authors were all rescaled in an identical way to our own data, i.e., also using the Portia group phase curve of Karkoschka (2001) for their respective Sun–Neptune-observer phase angles. Note that the geometric albedos (i.e., the albedo at zero phase angle) reported here differ from those reported by Dumas et al. (2002, 2003) because those authors did not make any phase angle correction. We follow the procedure in Paradis et al. (2019, 2023) and summarized in Appendix to determine this correction. All the error bars on geometric albedos given in Table 2 and Fig. 3 were linearly rescaled from the I/F errors, also described in Appendix.

There is statistically high-confidence evidence ($\gtrsim 2.5\sigma$) for spectral reddening between 0.5 and 1.6 μm for Galatea, Larissa, Despina, and Proteus, consistent with the spectra of Puck and Portia (Dumas et al., 2003), and the majority of previous observations of the neptunian satellites (see Table 2 for references); such a reddening may be caused by the presence of organic material (Trilling and Brown, 2000). Naiad appears to have a lower albedo than the other four moons.

While the K-band measurements of Proteus display a large scatter, there is some evidence that Proteus's albedo darkens from 1.87 to 2.4 μm, in stark contrast with the surfaces of Puck and Portia, which brighten from 1.6 to 2.4 μm (Paradis et al., 2023). The H-to-K-band brightening on Puck and Portia has been taken as evidence of the absence of a global layer of water-ice (Gibbard et al., 2005; Paradis et al., 2023), and a darkening could indicate the presence of water ice on Proteus, although this feature can also be matched by laboratory spectra of methane or HCN ice (Dumas et al., 2003). The similarity in infrared color between the four moons in this study may point to similar formation and evolution pathways for those moons, but additional near- and mid-infrared observations are required to constrain their compositions, with implications for their formation and subsequent evolution.

4. Conclusion

We have presented H-band reflectivity (I/F) measurements for the Neptunian moons Proteus, Galatea, Larissa, Despina, and Naiad obtained using the NIRC2 instrument at Keck Observatory. Taken in conjunction with literature measurements at other wavelengths, the reflectivities we derive show that the four larger satellites, excluding Naiad, appear to be slightly red from visible to infrared wavelengths,

Table 2
Available photometric information for the five satellites considered in this study.

Moon	Wavelength [μm]	Phase angle [°]	I/F	Geometric albedo	Reference
Proteus	0.5	15	0.037 ± 0.0024	0.096 ± 0.0062	Karkoschka (2003)
	1.1	0.7	0.072 ± 0.006	0.081 ± 0.0068	Dumas et al. (2003)
	1.26	1.29	0.026 ± 0.005	0.032 ± 0.0062	Trilling and Brown (2000)
	1.6	0.7	0.084 ± 0.002	0.095 ± 0.0023	Dumas et al. (2003)
	1.6	0.74	0.11 ± 0.0104	0.13 ± 0.012	This work
	1.6	1.29	0.028 ± 0.006	0.034 ± 0.0073	Trilling and Brown (2000)
	1.6	1.8	0.080 ± 0.016	0.11 ± 0.021	Molter et al. (2019)
	1.6	1.2	0.073 ± 0.016	0.09 ± 0.020	Molter et al. (2019)
	1.87	1.9	0.094 ± 0.011	0.13 ± 0.015	Dumas et al. (2002)
	2.04	0.7	0.075 ± 0.01	0.085 ± 0.011	Dumas et al. (2003)
	2.2	0.83	0.058 ± 0.016	0.069 ± 0.019	Roddier et al. (1997)
	2.2	1.8	0.092 ± 0.018	0.12 ± 0.023	Molter et al. (2019)
	2.2	1.2	0.10 ± 0.033	0.12 ± 0.041	Molter et al. (2019)
	2.2	1.29	0.047 ± 0.014	0.058 ± 0.017	Trilling and Brown (2000)
	2.37	0.7	0.065 ± 0.018	0.073 ± 0.020	Dumas et al. (2003)
Despina	0.5	15	0.035 ± 0.028	0.090 ± 0.0072	Karkoschka (2003)
	1.6	0.74	0.11 ± 0.011	0.13 ± 0.013	This work
	1.87	1.9	0.058 ± 0.036	0.08 ± 0.05	Dumas et al. (2002)
Galatea	0.5	15	0.031 ± 0.0028	0.079 ± 0.0072	Karkoschka (2003)
	1.6	1.66	0.088 ± 0.012	0.12 ± 0.016	de Pater et al. (2005)
	1.6	0.74	0.11 ± 0.0099	0.13 ± 0.012	This work
	1.87	1.9	0.086 ± 0.061	0.12 ± 0.08	Dumas et al. (2002)
	2.1	0.165	0.096 ± 0.015	0.12 ± 0.018	de Pater et al. (2005)
	2.1	1.66	0.094 ± 0.011	0.12 ± 0.014	de Pater et al. (2005)
Larissa	0.5	15	0.035 ± 0.0022	0.091 ± 0.0056	Karkoschka (2003)
	1.6	0.74	0.11 ± 0.0096	0.13 ± 0.011	This work
	1.87	1.9	0.079 ± 0.022	0.11 ± 0.03	Dumas et al. (2002)
Naiad	0.5	15	0.028 ± 0.0050	0.072 ± 0.013	Karkoschka (2003)
	1.6	0.74	0.061 ± 0.0072	0.071 ± 0.0083	This work

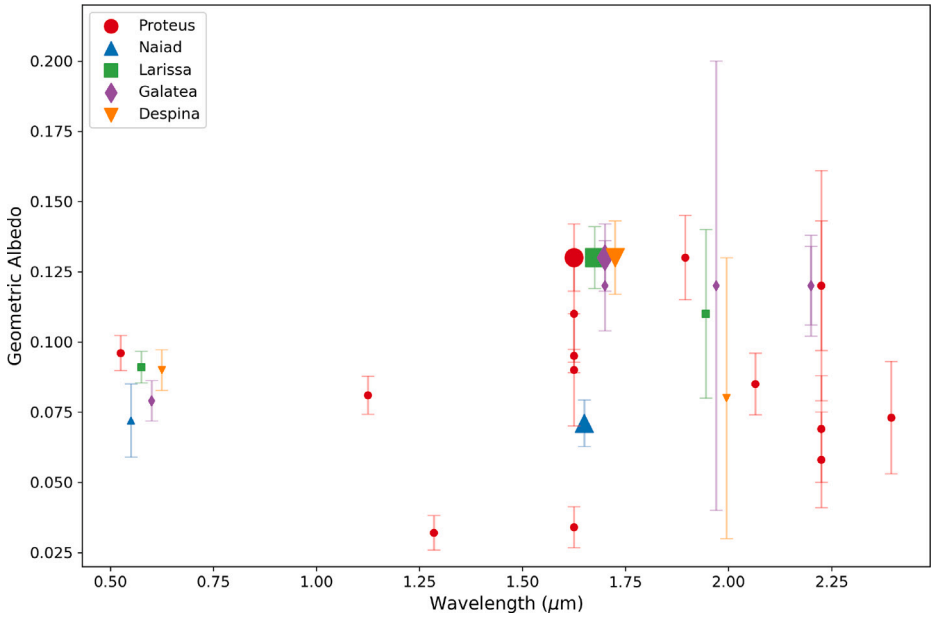

Fig. 3. Color information for Neptune's small regular satellites. Wavelengths have been offset slightly for better visualization of the error bars. Data from this work are highlighted with larger markers. See Table 2 for references. (For interpretation of the references to color in this figure legend, the reader is referred to the web version of this article.)

perhaps indicating the presence of organic material on their surfaces. We encourage using the James Webb Space Telescope (JWST) to obtain near- and mid-infrared spectra to constrain the composition of the moons.

CRediT authorship contribution statement

Mallory Helfenbein: Formal analysis, Investigation, Visualization, Writing – original draft, Writing – review & editing. **Edward M. Molter:** Conceptualization, Data curation, Investigation, Methodology, Software, Supervision, Visualization, Writing – review & editing. **Imke de Pater:** Data curation, Project administration, Supervision, Validation, Writing – review & editing, Investigation, Visualization. **Damya Souami:** Data curation, Investigation, Validation, Writing – review & editing.

Declaration of competing interest

The authors declare that they have no known competing financial interests or personal relationships that could have appeared to influence the work reported in this paper.

Data availability

The data is public.

Acknowledgments

The data presented herein were obtained at the W. M. Keck Observatory, which is operated as a scientific partnership among the California Institute of Technology, the University of California and the National Aeronautics and Space Administration. The Observatory was made possible by the generous financial support of the W. M. Keck Foundation, United States. The authors wish to recognize and acknowledge the very significant cultural role and reverence that the summit of Maunakea has always had within the indigenous Hawaiian community. We are most fortunate to have the opportunity to conduct observations from this mountain.

Mallory Helfenbein was participating through the Undergraduate Research Apprentice Program (URAP) at UC Berkeley.

Damya Souami thanks the France-USA Fulbright commission for supporting her visit at UC Berkeley as a Fulbright Scholar (2022–2023).

This work made use of Astropy,[4] a community-developed core Python package and an ecosystem of tools and resources for astronomy (Astropy Collaboration et al., 2013, 2018, 2022).

Facilities

Keck:NIRC2

Software

Astropy (Astropy Collaboration et al., 2013, 2018, 2022), matplotlib (Hunter, 2007), numpy (Harris et al., 2020), photutils (Bradley et al., 2022), shift_stack_moons (Molter, 2023)

Appendix. Flux bootstrapping method and error calculation

We used a flux bootstrapping method similar to that used by Gibbard et al. (2005), de Pater et al. (2014), Molter et al. (2019) and Paradis et al. (2023) in order to estimate the total flux density of each moon. Because of the substantial scattered light background, only the flux density from the core of the PSF of each moon could be reliably measured; therefore, to account for the missing flux density in the PSF sidelobes, we re-scaled the moons' values based on the sidelobes of the standard star FS2. We used 5 inner aperture radii from 8 to 12 pixels, and an outer (background) aperture radius of 18 pixels. We then determined the additional uncertainty on the flux densities from this bootstrapping technique by taking the standard deviation from these 5 different apertures. The reader is referred to the above references for more details. The overall I/F error is dominated by the combination of the flux calibration uncertainty (assumed to be 10%) and this flux bootstrapping error, and not by the RMS noise in the images (even for Naiad), which is why Naiad's relative flux uncertainty is no larger than the other moons. The signal-to-noise ratio of each moon is shown in Table 1, calculated by taking the ratio of the moon's flux density to its uncertainty due only to the RMS noise in the image. The RMS noise was determined in an annulus around the moon (with an inner radius large enough to exclude the PSF wings). The uncertainty in the moon's flux density due to this noise was calculated by multiplying the RMS noise by the square root of the number of pixels used to extract the moon's flux. The total uncertainty in each moon's flux density is then calculated by adding this RMS noise contribution, the flux bootstrapping error and the calibration uncertainty in quadrature.

[4] http://www.astropy.org.

References

Astropy Collaboration, Price-Whelan, A.M., Lim, P.L., Earl, N., Starkman, N., Bradley, L., Shupe, D.L., Patil, A.A., Corrales, L., Brasseur, C.E., Nöthe, M., Donath, A., Tollerud, E., Morris, B.M., Ginsburg, A., Vaher, E., Weaver, B.A., Tocknell, J., Jamieson, W., van Kerkwijk, M.H., Robitaille, T.P., Merry, B., Bachetti, M., Günther, H.M., Aldcroft, T.L., Alvarado-Montes, J.A., Archibald, A.M., Bódi, A., Bapat, S., Barentsen, G., Bazán, J., Biswas, M., Boquien, M., Burke, D.J., Cara, D., Cara, M., Conroy, K.E., Conseil, S., Craig, M.W., Cross, R.M., Cruz, K.L., D'Eugenio, F., Dencheva, N., Devillepoix, H.A.R., Dietrich, J.P., Eigenbrot, A.D., Erben, T., Ferreira, L., Foreman-Mackey, D., Fox, R., Freij, N., Garg, S., Geda, R., Glattly, L., Gondhalekar, Y., Gordon, K.D., Grant, D., Greenfield, P., Groener, A.M., Guest, S., Gurovich, S., Handberg, R., Hart, A., Hatfield-Dodds, Z., Homeier, D., Hosseinzadeh, G., Jenness, T., Jones, C.K., Joseph, P., Kalmbach, J.B., Karamehmetoglu, E., Kałuszyński, M., Kelley, M.S.P., Kern, N., Kerzendorf, W.E., Koch, E.W., Kulumani, S., Lee, A., Ly, C., Ma, Z., MacBride, C., Maljaars, J.M., Muna, D., Murphy, N.A., Norman, H., O'Steen, R., Oman, K.A., Pacifici, C., Pascual, S., Pascual-Granado, J., Patil, R.R., Perren, G.I., Pickering, T.E., Rastogi, T., Roulston, B.R., Ryan, D.F., Rykoff, E.S., Sabater, J., Sakurikar, P., Salgado, J., Sanghi, A., Saunders, N., Savchenko, V., Schwardt, L., Seifert-Eckert, M., Shih, A.Y., Jain, A.S., Shukla, G., Sick, J., Simpson, C., Singanamalla, S., Singer, L.P., Singhal, J., Sinha, M., Sipőcz, B.M., Spitler, L.R., Stansby, D., Streicher, O., Šumak, J., Swinbank, J.D., Taranu, D.S., Tewary, N., Tremblay, G.R., de Val-Borro, M., Van Kooten, S.J., Vasović, Z., Verma, S., de Miranda Cardoso, J.V., Williams, P.K.G., Wilson, T.J., Winkel, B., Wood-Vasey, W.M., Xue, R., Yoachim, P., Zhang, C., Zonca, A., Astropy Project Contributors, 2022. Astrophys. J. 935 (2), 167. http://dx.doi.org/10.3847/1538-4357/ac7c74.

Astropy Collaboration, Price-Whelan, A.M., Sipőcz, B.M., Günther, H.M., Lim, P.L., Crawford, S.M., Conseil, S., Shupe, D.L., Craig, M.W., Dencheva, N., Ginsburg, A., VanderPlas, J.T., Bradley, L.D., Pérez-Suárez, D., de Val-Borro, M., Aldcroft, T.L., Cruz, K.L., Robitaille, T.P., Tollerud, E.J., Ardelean, C., Babej, T., Bach, Y.P., Bachetti, M., Bakanov, A.V., Bamford, S.P., Barentsen, G., Barmby, P., Baumbach, A., Berry, K.L., Biscani, F., Boquien, M., Bostroem, K.A., Bouma, L.G., Brammer, G.B., Bray, E.M., Breytenbach, H., Buddelmeijer, H., Burke, D.J., Calderone, G., Cano Rodríguez, J.L., Cara, M., Cardoso, J.V.M., Cheedella, S., Copin, Y., Corrales, L., Crichton, D., D'Avella, D., Deil, C., Depagne, E., Dietrich, J.P., Donath, A., Droettboom, M., Earl, N., Erben, T., Fabbro, S., Ferreira, L.A., Finethy, T., Fox, R.T., Garrison, L.H., Gibbons, S.L.J., Goldstein, D.A., Gommers, R., Greco, J.P., Greenfield, P., Groener, A.M., Grollier, F., Hagen, A., Hirst, P., Homeier, D., Horton, A.J., Hosseinzadeh, G., Hu, L., Hunkeler, J.S., Ivezić, Ž., Jain, A., Jenness, T., Kanarek, G., Kendrew, S., Kern, N.S., Kerzendorf, W.E., Khvalko, A., King, J., Kirkby, D., Kulkarni, A.M., Kumar, A., Lee, A., Lenz, D., Littlefair, S.P., Ma, Z., Macleod, D.M., Mastropietro, M., McCully, C., Montagnac, S., Morris, B.M., Mueller, M., Mumford, S.J., Muna, D., Murphy, N.A., Nelson, S., Nguyen, G.H., Ninan, J.P., Nöthe, M., Ogaz, S., Oh, S., Parejko, J.K., Parley, N., Pascual, S., Patil, R., Patil, A.A., Plunkett, A.L., Prochaska, J.X., Rastogi, T., Reddy Janga, V., Sabater, J., Sakurikar, P., Seifert, M., Sherbert, L.E., Sherwood-Taylor, H., Shih, A.Y., Sick, J., Silbiger, M.T., Singanamalla, S., Singer, L.P., Sladen, P.H., Sooley, K.A., Sornarajah, S., Streicher, O., Teuben, P., Thomas, S.W., Tremblay, G.R., Turner, J.E.H., Terrón, V., van Kerkwijk, M.H., de la Vega, A., Watkins, L.L., Weaver, B.A., Whitmore, J.B., Woillez, J., Zabalza, V., Astropy Contributors, 2018. Astron. J. 156 (3), 123. http://dx.doi.org/10.3847/1538-3881/aabc4f.

Astropy Collaboration, Robitaille, T.P., Tollerud, E.J., Greenfield, P., Droettboom, M., Bray, E., Aldcroft, T., Davis, M., Ginsburg, A., Price-Whelan, A.M., Kerzendorf, W.E., Conley, A., Crighton, N., Barbary, K., Muna, D., Ferguson, H., Grollier, F., Parikh, M.M., Nair, P.H., Unther, H.M., Deil, C., Woillez, J., Conseil, S., Kramer, R., Turner, J.E.H., Singer, L., Fox, R., Weaver, B.A., Zabalza, V., Edwards, Z.I., Azalee Bostroem, K., Burke, D.J., Casey, A.R., Crawford, S.M., Dencheva, N., Ely, J., Jenness, T., Labrie, K., Lim, P.L., Pierfederici, F., Pontzen, A., Ptak, A., Refsdal, B., Servillat, M., Streicher, O., 2013. Astron. Astrophys. 558, A33. http://dx.doi.org/10.1051/0004-6361/201322068.

Banfield, D., Murray, N., 1992. Icarus 99 (2), 390–401.

Bradley, L., Sipőcz, B., Robitaille, T., Tollerud, E., Vinícius, Z., Deil, C., Barbary, K., Wilson, T.J., Busko, I., Donath, A., Günther, H.M., Cara, M., Lim, P.L., Meßlinger, S., Conseil, S., Bostroem, A., Droettboom, M., Bray, E.M., Bratholm, L.A., Barentsen, G., Craig, M., Rathi, S., Pascual, S., Perren, G., Georgiev, I.Y., de Val-Borro, M., Kerzendorf, W., Bach, Y.P., Quint, B., Souchereau, H., 2022. Astropy/Photutils: 1.4.0, 1.4.0. Zenodo, http://dx.doi.org/10.5281/zenodo.6385735.

Colas, F., Buil, C., 1992. Astron. Astrophys. 262 (1), L13.

Colina, L., Bohlin, R.C., Castelli, F., 1996. Astron. J. 112, 307. http://dx.doi.org/10.1086/118016.

de Pater, I., Davies, A.G., McGregor, A., Trujillo, C., Ádámkovics, M., Veeder, G.J., Matson, D.L., Leone, G., 2014. Icarus 242, 379–395. http://dx.doi.org/10.1016/j.icarus.2014.06.019.

de Pater, I., Gibbard, S.G., Chiang, E., Hammel, H.B., Macintosh, B., Marchis, F., Martin, S.C., Roe, H.G., Showalter, M., 2005. Icarus 174 (1), 263–272. http://dx.doi.org/10.1016/j.icarus.2004.10.020.

Déau, E., Dones, L., Rodriguez, S., Charnoz, S., Brahic, A., 2009. Planet. Space Sci. 57 (11), 1282–1301. http://dx.doi.org/10.1016/j.pss.2009.05.005.

Dumas, C., Smith, B.A., Terrile, R.J., 2003. Astron. J. 126 (2), 1080–1085. http://dx.doi.org/10.1086/375909.
Dumas, C., Terrile, R.J., Smith, B.A., Schneider, G., 2002. Astron. J. 123 (3), 1776–1783. http://dx.doi.org/10.1086/339022.
Gibbard, S.G., de Pater, I., Hammel, H.B., 2005. Icarus 174 (1), 253–262. http://dx.doi.org/10.1016/j.icarus.2004.09.008.
Ginsburg, A., Sipőcz, B.M., Brasseur, C.E., Cowperthwaite, P.S., Craig, M.W., Deil, C., Guillochon, J., Guzman, G., Liedtke, S., Lian Lim, P., Lockhart, K.E., Mommert, M., Morris, B.M., Norman, H., Parikh, M., Persson, M.V., Robitaille, T.P., Segovia, J.-C., Singer, L.P., Tollerud, E.J., de Val-Borro, M., Valtchanov, I., Woillez, J., Astroquery Collaboration, a subset of astropy Collaboration, 2019. Astron. J. 157 (3), 98. http://dx.doi.org/10.3847/1538-3881/aafc33.
Giorgini, J., 2011. In: Capitaine, N. (Ed.), Journées 2010: Systémes De Rèférence Spatio-Temporels. p. 87.
Giuliatti Winter, S.M., Madeira, G., Sfair, R., 2020. Mon. Not. R. Astron. Soc. 496 (1), 590–597. http://dx.doi.org/10.1093/mnras/staa1519.
Goldreich, P., Peale, S., 1966. Astron. J. 71, 425. http://dx.doi.org/10.1086/109947.
Goldreich, P., Tremaine, S., Borderies, N., 1986. Astron. J. 92, 490–494. http://dx.doi.org/10.1086/114178.
Hammel, H.B., Baines, K.H., Bergstralh, J.T., 1989. Icarus 80 (2), 416–438. http://dx.doi.org/10.1016/0019-1035(89)90149-8.
Harris, C.R., Millman, K.J., van der Walt, S.J., Gommers, R., Virtanen, P., Cournapeau, D., Wieser, E., Taylor, J., Berg, S., Smith, N.J., Kern, R., Picus, M., Hoyer, S., van Kerkwijk, M.H., Brett, M., Haldane, A., del Río, J.F., Wiebe, M., Peterson, P., Gérard-Marchant, P., Sheppard, K., Reddy, T., Weckesser, W., Abbasi, H., Gohlke, C., Oliphant, T.E., 2020. Nature 585 (7825), 357–362. http://dx.doi.org/10.1038/s41586-020-2649-2.
Hawarden, T.G., Leggett, S.K., Letawsky, M.B., Ballantyne, D.R., Casali, M.M., 2001. Mon. Not. R. Astron. Soc. 325 (2), 563–574. http://dx.doi.org/10.1046/j.1365-8711.2001.04460.x.
Hunter, J.D., 2007. Comput. Sci. Eng. 9 (3), 90–95. http://dx.doi.org/10.1109/MCSE.2007.55.
Jacobson, R.A., 1990. Astron. Astrophys. 231 (1), 241–250.
Karkoschka, E., 2001. Icarus 151 (1), 51–68. http://dx.doi.org/10.1006/icar.2001.6596.
Karkoschka, E., 2003. Icarus 162 (2), 400–407. http://dx.doi.org/10.1016/S0019-1035(03)00002-2.
Molter, N., 2023. Emolter/Shift_Stack_Moons: Mab Paper 0.0.6. Zenodo, http://dx.doi.org/10.5281/zenodo.7608459.
Molter, E., de Pater, I., Luszcz-Cook, S., Hueso, R., Tollefson, J., Alvarez, C., Sánchez-Lavega, A., Wong, M.H., Hsu, A.I., Sromovsky, L.A., Fry, P.M., Delcroix, M., Campbell, R., de Kleer, K., Gates, E., Lynam, P.D., Ammons, S.M., Coy, B.P., Duchene, G., Gonzales, E.J., Hirsch, L., Magnier, E.A., Ragland, S., Rich, R.M., Wang, F., 2019. Icarus 321, 324–345. http://dx.doi.org/10.1016/j.icarus.2018.11.018.
Namouni, F., Porco, C., 2002. Nature 417 (6884), 45–47. http://dx.doi.org/10.1038/417045a.
Owen, W.M., Vaughan, R.M., Synnott, S.P., 1991. Astron. J. 101, 1511. http://dx.doi.org/10.1086/115783.
Paradis, S., Moeckel, C., de Pater, I., 2023. Icarus 391, 115331. http://dx.doi.org/10.1016/j.icarus.2022.115331.
Paradis, S., Moeckel, C., Tollefson, J., de Pater, I., 2019. Astron. J. 158 (5), 178. http://dx.doi.org/10.3847/1538-3881/ab4264.
Peale, S.J., 1999. Annu. Rev. Astron. Astrophys. 37, 533–602. http://dx.doi.org/10.1146/annurev.astro.37.1.533.
Porco, C.C., 1991. Science 253 (5023), 995–1001. http://dx.doi.org/10.1126/science.253.5023.995.
Porco, C.C., West, R.A., McEwen, A., Del Genio, A.D., Ingersoll, A.P., Thomas, P., Squyres, S., Dones, L., Murray, C.D., Johnson, T.V., Burns, J.A., Brahic, A., Neukum, G., Veverka, J., Barbara, J.M., Denk, T., Evans, M., Ferrier, J.J., Geissler, P., Helfenstein, P., Roatsch, T., Throop, H., Tiscareno, M., Vasavada, A.R., 2003. Science 299 (5612), 1541–1547. http://dx.doi.org/10.1126/science.1079462.
Renner, S., Sicardy, B., Souami, D., Carry, B., Dumas, C., 2014. Astron. Astrophys. 563, A133. http://dx.doi.org/10.1051/0004-6361/201321910.
Roddier, F., Roddier, C., Brahic, A., Dumas, C., Graves, J.E., Northcott, M.J., Owen, T., 1997. Planet. Space Sci. 45 (8), 1031–1036. http://dx.doi.org/10.1016/S0032-0633(97)00026-3.
Salo, H., Hanninen, J., 1998. Science 282, 1102. http://dx.doi.org/10.1126/science.282.5391.1102.
Showalter, M., Lissauer, J.J., de Pater, I., French, R.S., 2017. AAS/Division for Planetary Sciences Meeting Abstracts #49. In: AAS/Division for Planetary Sciences Meeting Abstracts, Vol. 49, p. 104.01.
Smith, B.A., Soderblom, L.A., Banfield, D., Barnet, C., Basilevksy, A.T., Beebe, R.F., Bollinger, K., Boyce, J.M., Brahic, A., Briggs, G.A., Brown, R.H., Chyba, C., Collins, S.A., Colvin, T., Cook, A.F., Crisp, D., Croft, S.K., Cruikshank, D., Cuzzi, J.N., Danielson, G.E., Davies, M.E., de Jong, E., Dones, L., Godfrey, D., Goguen, J., Grenier, I., Haemmerle, V.R., Hammel, H., Hansen, C.J., Helfenstein, C.P., Howell, C., Hunt, G.E., Ingersoll, A.P., Johnson, T.V., Kargel, J., Kirk, R., Kuehn, D.I., Limaye, S., Masursky, H., McEwen, A., Morrison, D., Owen, T., Owen, W., Pollack, J.B., Porco, C.C., Rages, K., Rogers, P., Rudy, D., Sagan, C., Schwartz, J., Shoemaker, E.M., Showalter, M., Sicardy, B., Simonelli, D., Spencer, J., Sromovsky, L.A., Stoker, C., Strom, R.G., Suomi, V.E., Synott, S.P., Terrile, R.J., Thomas, P., Thompson, W.R., Verbiscer, A., Veverka, J., 1989. Science 246 (4936), 1422–1449. http://dx.doi.org/10.1126/science.246.4936.1422.
Smith, B.A., Soderblom, L.A., Beebe, R., Boyce, J., Briggs, G., Carr, M., Collins, S.A., Cook, I., Danielson, G.E., Davies, M.E., Hunt, G.E., Ingersoll, A., Johnson, T.V., Masursky, H., McCauley, J., Morrison, D., Owen, T., Sagan, C., Shoemaker, E.M., Strom, R., Suomi, V.E., Veverka, J., 1979. Science 206 (4421), 927–950. http://dx.doi.org/10.1126/science.206.4421.927.
Souami, D., Renner, S., Sicardy, B., Langlois, M., Carry, B., Delorme, P., Golaszewska, P., 2022. Astron. Astrophys. 657, A134. http://dx.doi.org/10.1051/0004-6361/202141598.
Thomas, P.C., Burns, J.A., Rossier, L., Simonelli, D., Veverka, J., Chapman, C.R., Klaasen, K., Johnson, T.V., Belton, M.J.S., Galileo Solid State Imaging Team, 1998. Icarus 135 (1), 360–371. http://dx.doi.org/10.1006/icar.1998.5976.
Thomas, P., Veverka, J., 1991. J. Geophys. Res. 96, 19261–19268. http://dx.doi.org/10.1029/91JA01461.
Tiscareno, M.S., Murray, C.D., 2018. Planetary ring systems. properties, structure, and evolution. http://dx.doi.org/10.1017/9781316286791.
Trilling, D.E., Brown, R.H., 2000. Icarus 148 (1), 301–306. http://dx.doi.org/10.1006/icar.2000.6505.
van Dam, M.A., Le Mignant, D., Macintosh, B.A., 2004. Appl. Opt. 43 (29), 5458–5467. http://dx.doi.org/10.1364/AO.43.005458.
Wizinowich, P., Acton, D.S., Shelton, C., Stomski, P., Gathright, J., Ho, K., Lupton, W., Tsubota, K., Lai, O., Max, C., Brase, J., An, J., Avicola, K., Olivier, S., Gavel, D., Macintosh, B., Ghez, A., Larkin, J., 2000. Publ. Astron. Soc. Pac. 112 (769), 315–319. http://dx.doi.org/10.1086/316543.
Wizinowich, P.L., Le Mignant, D., Bouchez, A., Chin, J., Contos, A., Hartman, S., Johansson, E., Lafon, R., Neyman, C., Stomski, P., Summers, D., van Dam, M.A., 2004. In: Bonaccini Calia, D., Ellerbroek, B.L., Ragazzoni, R. (Eds.), Advancements in Adaptive Optics. In: Society of Photo-Optical Instrumentation Engineers (SPIE) Conference Series, Vol. 5490, pp. 1–11. http://dx.doi.org/10.1117/12.552489.
Zhang, K., Hamilton, D.P., 2007. Icarus 188 (2), 386–399. http://dx.doi.org/10.1016/j.icarus.2006.12.002.
Zhang, K., Hamilton, D.P., 2008. Icarus 193 (1), 267–282. http://dx.doi.org/10.1016/j.icarus.2007.08.024.